First-Principles Study of Electron Transport through the Single-Molecule Magnet Mn_{12}

Salvador Barraza-Lopez,[1,*] Kyungwha Park,[1] Víctor García-Suárez,[2] and Jaime Ferrer[3]

[1]*Department of Physics, Virginia Polytechnic Institute and State University, Blacksburg Virginia, 24061, USA*
[2]*Department of Physics, Lancaster University, Lancaster, LA1 4YB, United Kingdom*
[3]*Departamento de Fisica, Universidad de Oviedo & CINN, 33007 Oviedo, Spain*

(Received 24 March 2009; published 18 June 2009)

We examine electron transport through a single-molecule magnet Mn_{12} bridged between Au electrodes using the first-principles method. We find crucial features which were inaccessible in model Hamiltonian studies: spin filtering and a strong dependence of charge distribution on local environments. The spin filtering remains robust with different molecular geometries and interfaces, and strong electron correlations, while the charge distribution over the Mn_{12} strongly depends on them. We point out a qualitative difference between locally charged and free-electron-charged Mn_{12}.

DOI: 10.1103/PhysRevLett.102.246801 PACS numbers: 85.65.+h, 75.50.Xx, 85.75.−d, 73.23.Hk

In the past two decades, electron transport through quantum dots has been studied in single-electron transistors as an effort to manipulate single electrons at a time [1–3]. Semiconducting quantum dots were typically used because of easy manipulation of the number of electrons inside the dots, by varying gate voltages.

Recently, several experiments [4–7] on electron transport through a single-molecule magnet (SMM) Mn_{12} were reported in transistor setups or scanning tunneling microscope (STM) measurements. SMMs differ from magnetic clusters or quantum dots in the sense that transition metal ions in SMMs are interacting with each other via superexchange through ligands, and that there is large magnetic anisotropy caused by spin-orbit coupling within each SMM. Thus, the degeneracy in different magnetic states for a given spin multiplet of SMMs is lifted even in the absence of external magnetic field. The main questions in these transport studies are whether the electronic and magnetic properties of SMMs would survive in low-dimensional structures and how the magnetic degrees of freedom interplay with the electronic degrees of freedom. The challenges in these types of experiments are, so far, to maintain stable molecular structures [8], to determine orientations of SMMs relative to surfaces, and to characterize interfaces.

Our previous first-principles studies [9–11] showed that SMMs are weakly coupled to Au surfaces and electrodes. Thus, transport through SMMs belongs to a Coulomb blockade regime. In most theoretical studies on transport through SMMs, one treated SMMs as quantum dots and relied on many-body model Hamiltonians with unknown parameter values [12–17]. However, in contrast to quantum dots, the magnetic properties of SMMs are delicately balanced by interactions among transition metal ions. Thus, caution needs to be exercised in interpretation of the experimental data to construct effective model Hamiltonians.

In this Letter, we simulate semi-infinite electrodes and different molecular geometries and interfaces, and investigate transport properties through a SMM Mn_{12} bridged between Au electrodes, using the nonequilibrium Green's function method in conjunction with spin-polarized density-functional theory (DFT). Our calculations provide crucial microscopic information such as a spin-filtering effect and a strong dependence of charge distribution over the Mn_{12} on local environments. This information was unattainable in the theoretical studies solely based on model Hamiltonians with unknown parameter values, and could qualitatively change transport properties through SMMs. Mn_{12} molecules used in the transport experiments [4,7] were bulky due to large ligands, and so the distances between the Mn_{12} molecule and the electrodes (or the lengths of linker molecules) for our molecular geometries are comparable to or much shorter than those in the experiments. We emphasize the effects of interfaces and molecular geometries on the charge distribution and the coupling constant between a SMM and electrodes. To take into account strong electron correlations in transition metal ions, we included a Hubbard-like U term in our previous calculations [10,11].

We consider two molecular geometries for a SMM Mn_{12} bridged between Au(111) electrodes as shown in Figs. 1(a) and 1(b): (i) geometry 1 where the magnetic easy axis of Mn_{12} is perpendicular to the transport direction and Mn_{12} is attached to the electrodes via alkane chains and S atoms. (ii) geometry 2 where the easy axis of Mn_{12} is parallel to the transport direction and Mn_{12} is attached to the electrodes via four S atoms. The linker molecules are used to chemically bind the Mn_{12} to the electrodes, and play a role of energy barriers whose heights depend on their lengths and types of chemical bonding. The Au electrodes are treated as semi-infinite and the scattering region contains a few Au layers, linker molecules, and Mn_{12}, as shown in Fig. 1. Our calculations are performed using SMEAGOL [18,19], a quantum transport code interfaced with DFT SIESTA program [20]. Generalized-gradient approximation (GGA) [21] is used for exchange-correlation potential in spin-polarized DFT formalism. When spin-orbit coupling is included self-consistently for an isolated neutral Mn_{12}

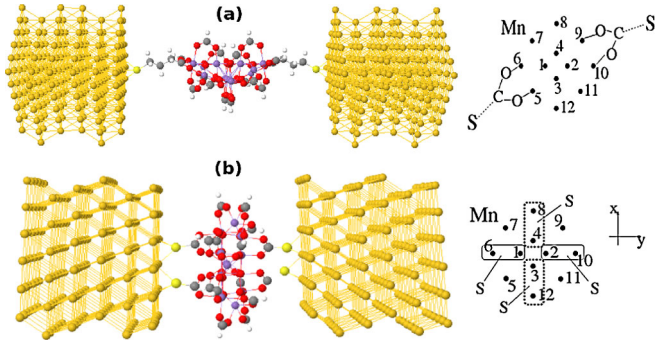

FIG. 1 (color online). Scattering region for (a) geometry 1 consisting of Mn_{12} attached to Au layers via S atoms and alkane chains (distance between the electrodes $d = 25.7$ Å), and for (b) geometry 2 consisting of Mn_{12}, four S atoms, and Au layers ($d = 14.5$ Å). The transport direction is along the horizontal axis, z axis. Semi-infinite Au electrodes are considered in calculations (not shown). On the right-hand side the positions of the Mn ions are marked for each geometry. For geometry 1 the dashed lines indicate the alkane chains. For geometry 2 the solid and dashed blocks represent the areas where the four S atoms are attached through bonding to the C atoms.

molecule, magnetic anisotropy barrier is computed to be 65.3 K using VASP [22] and 66.4 K using SIESTA [19], which agrees well with experimental data [23]. Gate voltages and interactions with phonons are not considered in this study. Further details of the method and assumptions for this work and brief discussion on the transport for geometry 1 were presented in Ref. [11].

The spin-polarized densities of states (DOS) of the scattering region projected onto all Mn d orbitals for geometries 1 and 2 are shown relative to the Fermi level, E_f, in Figs. 2(a) and 2(b). In the DOS for both geometries a bin size of 0.5 meV and Gaussian broadening of 1 meV are used. The minority-spin DOS become negligible in the energy window (−1.6, 0.42 eV) and (−1.5, 0.3 eV) relative to E_f for geometries 1 and 2, respectively. Thus, for both geometries only the majority-spin orbitals contribute to the densities near E_f. Further discussion of the DOS for geometry 1 is followed by that for geometry 2.

For geometry 1 the fourfold symmetry of Mn_{12} is broken due to the linker molecules so that the degeneracy in the molecular orbitals is lifted. As shown in Fig. 2(a), the projected densities of states (PDOS) for Mn(5) and Mn(9) completely differ from those for Mn(7) and Mn(11), although the four Mn sites are equivalent according to the fourfold symmetry. The individual molecular orbitals are clearly identifiable due to the larger distance between the Mn_{12} and the electrodes (or longer linker molecules) compared to those in geometry 2. The coupling (or broadening) of the orbitals to the electrodes near E_f is of the order of 1 meV or less. The lowest unoccupied molecular orbital (LUMO) is located slightly above E_f and the highest occupied molecular orbital (HOMO) is placed 0.29 eV below E_f [Fig. 2(a)]. The LUMO is mainly from two of the Mn ions in the outer ring, Mn(5) and Mn(9), while the HOMO is from Mn(8) and Mn(12).

For geometry 2 the shorter distance between the Mn_{12} and the electrodes allows the molecular orbitals to substantially broaden, which makes the individual orbitals unidentifiable [compare the insets of Figs. 2(a) and 2(b)]. That distance for geometry 2 is about a half of that for geometry 1, but the increase in the coupling constant for geometry 2 is much greater than a factor of 2 due to the exponential decay of the coupling with the distance for a given chemical bonding. The group of peaks near E_f is formed by broadening of the LUMO, which arises from coupling of all of the Mn ions to the electrodes, in contrast to the case of geometry 1. The HOMO broadens due to coupling of Mn(6), Mn(8), Mn(10), and Mn(12) to the electrodes. In geometry 2 the fourfold symmetry of an isolated Mn_{12} is, to some extent, preserved, because the linker molecules are attached in a fourfold symmetric fashion. The coupling constant between the Mn_{12} and electrodes near E_f is of the order of 10 meV [insets of Fig. 2(b)].

We compute a spin-polarized transmission coefficient $T(E)$ for geometry 1 and our result at zero bias is shown in Fig. 3(a). The majority-spin LUMO is responsible for the resonant tunneling near E_f. The widths of the $T(E)$ peaks,

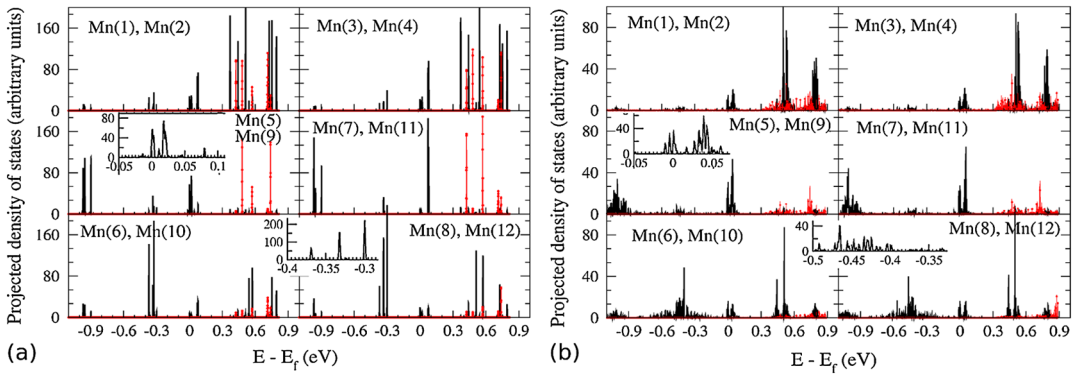

FIG. 2 (color online). Spin-polarized density of states (DOS) projected onto Mn d orbitals (a) for geometry 1 and (b) for geometry 2: majority spin (black), minority spin (red with symbol). Refer to Fig. 1 for numbering of the Mn ions. Insets: zoom-in of the majority DOS onto Mn(5), Mn(9), Mn(8), and Mn(12).

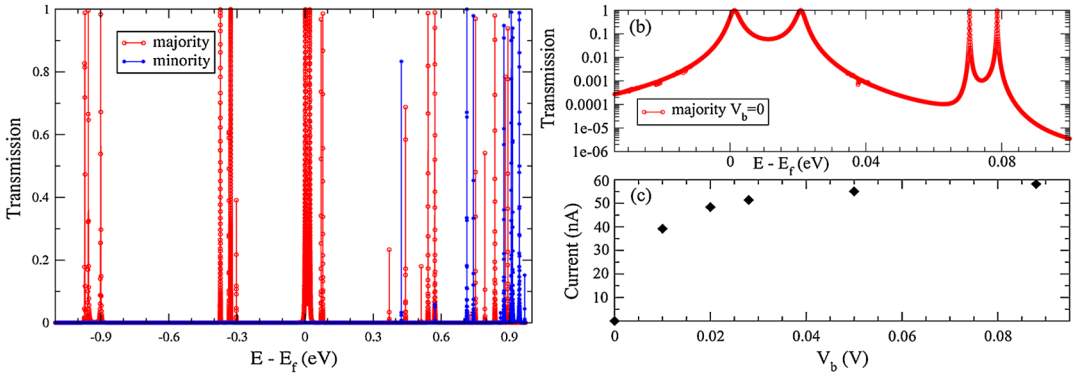

FIG. 3 (color online). (a) Spin-polarized transmission coefficient at zero bias, (b) zoom-in of the majority-spin transmission at zero bias [(a)], and (c) computed current I vs bias voltage V_b for geometry 1.

in general, depend on broadening of the orbitals, phonon populations, and defects. In our case, since we did not include defects or interactions with phonons, the widths depend on the broadening only. The weak coupling leads to the widths of the $T(E)$ peaks ranging from 0.01 to 1 meV [Fig. 3(b)]. The minority-spin contribution to $T(E)$ appears only 0.42 eV above E_f and 1.6 eV below E_f. This agrees with the locations of the orbitals in the PDOS [Fig. 2(a)]. For geometry 1 there is a one-to-one mapping between the $T(E)$ peaks and the orbitals. The spatially resolved density of states integrated over $(-0.23, 0.06$ eV) relative to E_f (Fig. 4) clearly corroborates that minority-spin electrons cannot tunnel through the Mn_{12} at low bias voltages. Using the same analogy, we expect that for geometry 2 only the majority-spin orbitals would contribute to $T(E)$ near E_f, and that the $T(E)$ peaks would be wider due to the broadening of the orbitals. As shown in Fig. 3(c), for geometry 1 our computed current as a function of bias voltage V_b is of the order of tens of nA when $V_b < 0.1$ V. For a given positive V_b, the chemical potential of the left (right) electrode increases (decreases) by $eV_b/2$. We find that for $0 < V_b < 0.1$ V, $T(E)$ is shifted upward compared to the zero-bias $T(E)$ without changing the main features. This shift is caused by the polarization of the Mn_{12} with V_b and the amount of the shift is proportional to V_b. Then the area of $T(E)$ integrated over E starts to saturate above 0.02 V, which results in the saturation in the current-voltage dependence [Fig. 3(c)].

To compare with experiment, additional electron correlations within the Mn ions that are absent in standard DFT must be considered. Beyond DFT, the U term was included in our calculation of the electronic structure of an isolated Mn_{12} molecule [10] using VASP. It was found that the majority-spin HOMO-LUMO gap increased to 1.1 eV and that the majority-spin LUMO was shifted upward by 0.12 eV. The minority-spin LUMO was, however, still 0.12 eV above the majority-spin LUMO. Thus, when an extra electron is added to the Mn_{12}, the majority-spin orbitals are still well separated from the minority-spin orbitals. Consequently, only majority-spin electrons can be tunneled through the Mn_{12} at low bias voltages (below 0.5 eV). Thus, we conclude that the spin-filtering effect remains robust with different molecular geometries and interfaces, and strong electron correlations.

Henceforth, we discuss a subtle but important issue in the transport through SMM Mn_{12}. The computed charging energy of an isolated Mn_{12} is 3.8 eV and thus the Mn_{12} can be only singly charged at low bias voltages. Because of the nature of less-than-half-filled d orbitals, the Mn d orbitals in the Mn_{12} are not spin degenerate. If an extra electron is

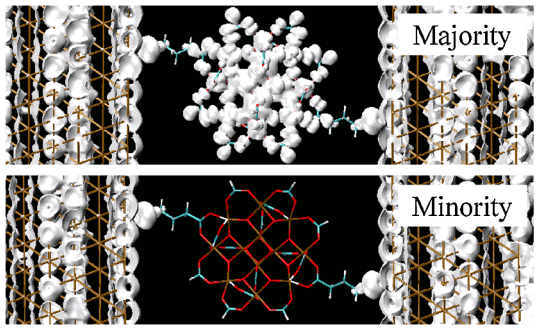

FIG. 4 (color online). Majority-spin and minority-spin density of states integrated between -0.23 and 0.06 eV relative to the Fermi level with isosurface criterion of 2 e/nm^3 for geometry 1.

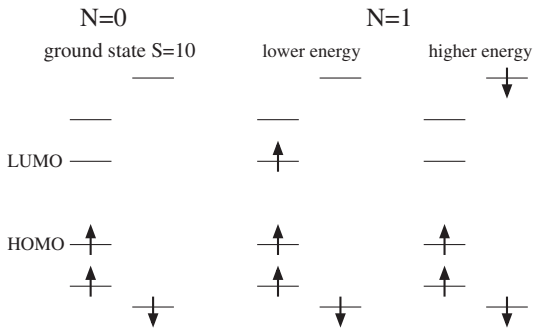

FIG. 5. Spin nondegenerate molecular orbitals of neutral Mn_{12} ($N = 0$) in the ground state ($S = 10$) and of singly charged Mn_{12} ($N = 1$) in the ground state and an excited state, obtained from DFT. In each state, four majority-spin (two minority-spin) orbitals are shown on the left (right).

added to Mn_{12}, the ground state would be achieved when the added electron has majority spin (Fig. 5). This is the origin of the spin-filtering effect in the transport through Mn_{12}. However, this argument must not be straightforwardly interpreted that the ground-state spin of $[Mn_{12}]^{1-}$, is $S = 10 + 1/2 = 21/2$. This is true only if the ground-state spin of $[Mn_{12}]^{1-}$ has a collinear configuration or if the extra charge is distributed over several Mn sites instead of being localized at one Mn site.

When conduction electrons are added to the Mn_{12} from the electrodes, our DFT calculations with collinear spin configurations support that the electrons will be distributed over more than one Mn site. The specific distribution of the electrons over the Mn sites depends on the way the Mn_{12} molecule is attached to the electrodes. For geometry 1 the electrons will be mainly distributed over the Mn(5) and Mn(9) sites, while for geometry 2 they will be distributed over all of the Mn sites [Figs. 2(a) and 2(b)]. Our noncollinear DFT calculations on $[Mn_{12}]^{1-}$ (using SIESTA) reveal that the collinear spin configuration with $S = 21/2$ has the lowest energy.

Some transport studies based on model Hamiltonians, [4,13,16] assumed that a singly charged Mn_{12} molecule has the ground-state spin of $S = 19/2$, by referring to experiments [24,25] performed on locally charged Mn_{12} molecules. In these experiments, extra electrons were added to the magnetic core of the Mn_{12}, by inserting cations (or electron donors) close to 1 or two of the Mn ions. Since a bulk form of Mn_{12} molecules is an insulator, the added electrons would be localized to the Mn sites closest to the cations. The experiments showed that the total spin for $[Mn_{12}]^{-1}$ was $S = 19/2$, and that one of the Mn ions in the outer ring changed its valence from 3+ ($S = 2$) to 2+ ($S = 5/2$). In contrast to typical quantum dots, the total spin of Mn_{12} is maintained through delicate balance among interactions between the different Mn ions. We perform noncollinear calculations on $Mn_{11}Fe$ (one of the Mn ions in the outer ring is replaced by Fe in the Mn_{12} geometry) in order to mimic a singly locally charged Mn_{12}. Using $U_{Mn} = 4$ eV [10] and $U_{Fe} = 6$ eV in VASP, we find that the collinear spin configuration with $2S = 19$ has 100 meV higher energy than the collinear spin configuration with $2S = 21$. But the latter has 5.8 meV higher energy than the noncollinear spin configuration ($2S = 18.71$) in which the magnetic moment vector of the Fe^{3+} ($S = 5/2$) ion is tilted by 62° from the moment vectors of the 11 Mn ions mostly aligned along with the z axis. Additional noncollinear calculations on the $Mn_{11}Fe$ with $U = 0$ also supports that the collinear spin configuration with $2S = 21$ is not the ground state for the singly locally charged Mn_{12}. Thus, the spin-filtering effect and single-electron picture (Fig. 5) are compatible with the experimental findings [24,25].

In summary, we have investigated transport properties through a Mn_{12} molecule bridged between Au(111) electrodes using the nonequilibrium Green's function method and spin-polarized DFT. We found that the Mn_{12} functioned as a spin filter in a low bias regime (below 0.5 eV). The spin-filter effect persisted with different molecular geometries and interfaces and strong electron correlations, while the distribution of conduction electrons over the Mn_{12} strongly depended on them. Conduction electrons from the electrodes would be distributed over several Mn sites rather than being localized at one Mn site. There is no contradiction between the spin-filtering effect and the experimental observation on $S = 19/2$ for the singly locally charged Mn_{12} molecules.

K. P. was supported by NSF DMR-0804665, the Jeffress Memorial Trust Funds, and NCSA under DMR060009N. J. F. was supported by MEC FIS2006-12117. The authors are grateful to W. Wernsdorfer for discussions.

*Present address: School of Physics, Georgia Institute of Technology, Atlanta, GA 30332, USA.

[1] Y. Meir *et al.*, Phys. Rev. Lett. **66**, 3048 (1991).
[2] D. Goldhaber-Gordon *et al.*, Nature (London) **391**, 156 (1998).
[3] S. M. Cronenwett *et al.*, Science **281**, 540 (1998).
[4] H. B. Heersche *et al.*, Phys. Rev. Lett. **96**, 206801 (2006).
[5] M.-H. Jo *et al.*, Nano Lett. **6**, 2014 (2006).
[6] J. J. Henderson *et al.*, J. Appl. Phys. **101**, 09E102 (2007).
[7] S. Voss *et al.*, Phys. Rev. B **78**, 155403 (2008).
[8] A recent report [M. Mannini *et al.*, Nature Mater. **8**, 194 (2009)] on a thin film of SMMs Fe_4 showed a possibility of stabilization of SMMs on surfaces.
[9] S. Barraza-Lopez *et al.*, Phys. Rev. B **76**, 224413 (2007).
[10] S. Barraza-Lopez *et al.*, J. Appl. Phys. **103**, 07B907 (2008).
[11] S. Barraza-Lopez *et al.*, J. Appl. Phys. **105**, 07E309 (2009).
[12] G.-H. Kim and T.-S. Kim, Phys. Rev. Lett. **92**, 137203 (2004).
[13] C. Romeike *et al.*, Phys. Rev. Lett. **96**, 196805 (2006).
[14] M. N. Leuenberger and E. R. Mucciolo, Phys. Rev. Lett. **97**, 126601 (2006).
[15] F. Elste and C. Timm, Phys. Rev. B **73**, 235305 (2006).
[16] G. González *et al.*, Phys. Rev. B **78**, 054445 (2008).
[17] L. Michalak *et al.*, arXiv:0812.1058.
[18] A. R. Rocha *et al.*, Phys. Rev. B **73**, 085414 (2006).
[19] L. Fernández-Seivane *et al.*, J. Phys. Condens. Matter **18**, 7999 (2006).
[20] J. M. Soler *et al.*, J. Phys. Condens. Matter **14**, 2745 (2002); J. Junquera *et al.*, Phys. Rev. B **64**, 235111 (2001); P. Ordejón *et al.*, Phys. Rev. B **51**, 1456 (1995).
[21] J. P. Perdew *et al.*, Phys. Rev. Lett. **77**, 3865 (1996).
[22] G. Kresse and J. Furthmüller, Phys. Rev. B **54**, 11 169 (1996); G. Kresse and J. Furthmüller, Comput. Mater. Sci. **6**, 15 (1996).
[23] A. L. Barra *et al.*, Phys. Rev. B **56**, 8192 (1997); S. Hill *et al.*, Phys. Rev. Lett. **80**, 2453 (1998).
[24] H. J. Eppley *et al.*, J. Am. Chem. Soc. **117**, 301 (1995); M. Soler *et al.*, J. Am. Chem. Soc. **125**, 3576 (2003).
[25] R. Basler *et al.*, Inorg. Chem. **44**, 649 (2005).